Subpolar activation of halogen heterogeneous chemistry in austral spring

Brian Zambri[1], Douglas E. Kinnison[2], and Susan Solomon[1]

[1]Department of Earth, Atmospheric, and Planetary Sciences, Massachusetts Institute of Technology, Cambridge, MA, USA
[2]Atmospheric Chemistry Observations and Modeling Laboratory, National Center for Atmospheric Research, Boulder, CO, USA

Submitted to *Geophysical Research Letters*

July 2020

Revised November 2020

Key points:

- Observed and modeled NO_2 depletion indicates significant heterogeneous chemistry in the Southern Hemisphere springtime subpolar lower stratosphere.
- Novel evidence for chemical processes is revealed using probability distributions in NO_2 data versus simulations.

Correspondence to:
Brian Zambri
Department of Earth, Atmospheric, and Planetary Sciences
Massachusetts Institute of Technology
77 Massachusetts Avenue

Cambridge, MA 02139
Email: bzambri@mit.edu

ABSTRACT

Heterogeneous halogen chemistry plays a dominant role in driving changes in polar chemical composition and ozone depletion. Activation of halogens outside the polar regions may result in depletion of local ozone, along with changes in the chemical budgets of various species in the lower stratosphere (LS). In this paper, the means and distributions of NO_2 measurements from the Stratospheric Aerosol and Gas Experiment III (SAGE3m) are compared to simulations from a coupled climate-chemistry model, in order to better characterize and quantify subpolar heterogeneous halogen chemistry. NO_2 abundances from a simulation with heterogeneous chemistry are drawn from the same distribution as the SAGE3m observations, while the NO_2 distribution is different in a simulation without heterogeneous chemistry. Results indicate that heterogeneous chemistry plays a significant role in determining the chemical composition of the subpolar LS in austral spring and show how analysis of distribution functions can provide useful insights to chemical processes.

Plain Language Summary. Much research has been done on the impacts of ozone-depleting substances on the atmospheres of the polar regions, where their impacts, including the infamous Antarctic ozone hole, are greatest. However, it is possible for these same chemicals to be active outside the polar regions, where they can destroy ozone locally as they do near the poles. In this study, we analyze observations of NO_2 outside the polar region. Because its concentrations are also impacted by the same chemistry that destroys ozone, NO_2 is a good indicator of where chemistry involving ozone-depleting substances is occurring. We provide important evidence for the active presence of ozone-depleting substances outside of the polar regions. In addition, we use a model to show that the chemistry is essential to explain the observed NO_2 distributions. The

results presented here should motivate further research on the impacts of ozone-depleting substances on ozone abundances throughout the atmosphere.

1. Introduction

It is well known that heterogeneous halogen chemistry in and on polar stratospheric particles (PSCs) plays a dominant role in driving changes in polar chemical composition (e.g., ClO, HCl, $ClONO_2$, NO_2) and ozone depletion. While such processes could also be important outside the polar regions, their impacts there are smaller and therefore more difficult to identify (see, e.g., Solomon, 1999, and references therein). Significant activation of inorganic halogens outside the polar regions may potentially result in the following: (i) depletion of ozone, including possible chemistry-climate coupling (e.g., Anderson et al., 2017; Hanson et al., 1994), (ii) changes in the chemical budgets not only of chlorine and bromine species, but also those of nitrogen compounds in the upper troposphere and lower stratosphere (Adams et al., 2017; Solomon et al., 2016; Zambri et al., 2019); and (iii) alteration of the local loss rates and lifetimes of some organic molecules due to enhanced atomic chlorine concentrations, e.g., C_2H_6 and methane near the tropopause (Lelieveld et al., 1999). These considerations broaden the scope of potential impacts associated with the chemistry of the subpolar stratosphere.

Anderson et al. (2012, 2017) theorized potential roles of liquid sulfate aerosols for ozone loss under cold tropopause conditions at mid-latitudes along with changes in water vapor associated with deep convection. Solomon et al. (2016) used model calculations to argue that heterogeneous halogen activation may occur near the tropical monsoon regions as well. Near the mid-latitude tropopause, some modeling studies have suggested that heterogeneous chemistry might also occur on cirrus cloud particles (e.g., Borrmann et al., 1996; Solomon et al., 1997). A number of observational studies have made use of volcanic perturbations to provide airborne and/or satellite evidence for reductions in NO_x associated with liquid sulfate aerosol chemistry

(e.g., Adams et al., 2017; Fahey et al., 1993; Zambri et al., 2019) but the specific reactions involved and their chemical impacts are not fully established. Important evidence has been presented for heterogeneous halogen chemistry in the tropopause region outside the polar vortices, but its scope and impacts remain uncertain (e.g., Barrera et al., 2020; Santee et al., 2011; Thornton et al., 2003). For this reason, additional study, especially with satellite methods that can provide extensive temporal and latitudinal coverage, is useful.

In this study, we analyze the chemistry of the Southern Hemisphere (SH) subpolar lower stratosphere in September and October using satellite observations from the Stratospheric Aerosol and Gas Experiment III on the Meteor–3M satellite (SAGE3m) in conjunction with the National Center for Atmospheric Research (NCAR) Community Earth System Model, version 2 (CESM2) Whole Atmosphere Community Climate Model (WACCM6; Danabosoglu et al., 2020; Gettelman et al., 2019). The model is run in specified dynamics (SD) mode wherein an observations-based reanalysis provides the temperatures and winds that are important for the chemistry. NO_2 is a useful indicator of heterogeneous processes. Reactions on surfaces (Solomon et al., 2015) convert NO_2 from short-lived NO_x reservoir species to longer-lived reservoir species, thereby locally depleting NO_2 and "denoxifying" the atmosphere (Table S1). Some heterogeneous processes result only in denoxification (e.g., $N_2O_5 + H_2O \rightarrow 2HNO_3$) and indirectly affect halogens, while others not only denoxify but also directly activate halogens from longer-lived species to more reactive forms (e.g., $HCl+ClONO_2 \rightarrow HNO_3+Cl_2$). Therefore, NO_2 abundances are a key tool for analysis of heterogeneous processing and evaluation of chemical understanding. We show how comparisons of not just means but more importantly the modeled and observed NO_2 distributions, defined by their discrete probability density functions (PDF) can be expected to demonstrate *where, when, and by how much heterogeneous halogen chemistry can perturb chemical composition outside the*

polar vortex. The analysis of probability distributions is shown to be a useful tool, and can also be expected to improve understanding of the measurement capabilities (including sensitivity and precision).

2. Materials and Methods

2.1 SAGE3m

The SAGE III was launched aboard the Russian Aviation and Space Agency's Meteor–3M satellite (Mauldin et al., 1998). The satellite was launched on December 10, 2001 into a Sun-synchronous orbit at an altitude of 1020 km and with an approximate 9:00 a.m. equatorial crossing time on the ascending node. The occultation instrument provided NO_2 measurements are reported at 0.5-km intervals from the tropopause to 45 km from 2002 to 2005, mostly at high latitudes in the Northern Hemisphere (between 50° and 80°N) and midlatitudes in the Southern Hemisphere (between 30° and 50°S). SAGE3m NO_2 observations are interpolated vertically to the CESM2(WACCM) grid.

2.2 CESM2(WACCM)

The CESM2(WACCM6) is the latest version of the CESM (Danabosoglu et al., 2020; Gettelman et al., 2019). The configuration of CESM2(WACCM) used here features ~2º (1.9º latitude × 2.5º longitude) horizontal resolution and a finite volume dynamical core (Lin & Rood, 1997). The model was run in specified dynamics mode (WACCM–SD) using the National Aeronautics and Space Administration Global Modeling and Assimilation Office Modern-Era Retrospective analysis for Research and Applications, Version 2 (MERRA2) meteorological fields (Gelaro et al., 2017). WACCM–SD allows for the synoptic comparison of model and observations;

in particular, WACCM has a purpose-built capability to output chemical constituent and other information at the specific longitude, latitude, and local time of a given satellite instrument. This tool has been employed in previous studies, for example, to examine sunrise and sunset data for $ClONO_2$ and O_3 (Sakazaki et al., 2015; Solomon et al., 2015). We have leveraged this capability to extract the model output at the same times and locations as the SAGE3m observations, which allows for a like-like comparison of model and observations.

2.3 Defining the subpolar region

The stratospheric polar vortex is a large-scale region of air that is contained by strong westerly winds that circle the polar region. This westerly jet stream is usually referred to as the polar night jet. The polar vortex extends from the tropopause through the stratosphere and into the mesosphere (above 50 km; Waugh, Sobel & Polvani, 2017). Cold temperatures and low ozone abundances, relative to midlatitudes, are associated with the air inside the vortex, because the polar vortex inhibits the exchange of polar and midlatitude air (Fig. 1). The potential vorticity (PV) is a conserved quantity that acts as a tracer for motion on an isentropic surface and is frequently used to distinguish polar versus midlatitude airmasses, although the vortex is not completely impermeable. In the winter, the magnitude of the PV is larger at the pole than at midlatitudes. The spacing of PV contours is tightest at the polar vortex edge, and widens inside the vortex and at latitudes equatorward of the vortex edge. The edge of the vortex is therefore defined to be where the contours of PV are closest together, quantified as the location of the maximum PV gradient with respect to equivalent latitude (Nash et al., 1996). In order to identify activation of inorganic halogens and heterogeneous chemistry, we consider only profiles that are outside the vortex and within 8º of the polar vortex edge for a given day. Fig. 1 illustrates the selection of “subpolar”

SAGE3m retrievals for October 29, 2014. Examination of rates of chlorine activation in the model (not shown) indicate that sulfuric acid activation is more than 10x greater than nitric acid trihydrate activation in this region. The chlorine activation also shows a band of significant activation about 8–10º in the subpolar region, which motivates the choice of band width. Latitudes of profiles considered to be subpolar range from 44ºS to 58ºS, with a mean latitude of 52ºS. In addition, Fig. S1 shows that in a second, more equatorward 8º band (i.e., 9º–16º from the vortex edge), there is very little activation, as indicated by the much more comparable WACCMhet and WACCMnoHet distributions.

2.4 Comparison of observed and modelled NO_2 distributions

In order to compare the NO_2 distributions based on SAGE3m observations and the CESM2(WACCM) simulations with and without heterogeneous chemistry (WACCMhet; includes all heterogeneous reactions on natural, sulfate, and ice polar stratospheric clouds, and WACCMnoHet; all halogen heterogeneous reactions are zeroed), we use the two-sample Kolmogorov–Smirnov test (K–S test; Smirnov, 1948). The two-sample K–S statistic is given by

$$D = \max_x |F_1(x) - F_2(x)|\,, \tag{1}$$

where F_1 and F_2 are the empirical distribution functions (ECDF) of the respective samples. The K–S test measures the maximum distance between the empirical distributions; the two data samples are deemed to be drawn from different distributions (i.e., the null hypothesis rejected) at level α if the distance, D, is smaller than some critical value,

$$c(\alpha, n_1, n_2) = \frac{1}{\sqrt{n_1}} \cdot \sqrt{-\ln\left(\frac{\alpha}{2}\right) \cdot \frac{1 + \frac{n_2}{n_1}}{2n_2}}, \tag{2}$$

where n_1 and n_2 are the sample sizes. The K–S test statistic is illustrated in Fig. 2, which shows an example of distributions of NO_2 for SAGE3m (black), WACCMhet (blue), and WACCMnoHet (red), where vertical dashed lines indicate the different values of D. As discussed further below, in the UTLS region the polar vortex is not as strong a barrier between polar and subpolar air, and so we also include the results of a simulation in which the heterogeneous chemical reactions were turned off only poleward of 60ºN/S (WACCMnoHet60NS; green line in Figs. 2–3) to identify the extent to which mixing may impact the observed and modelled NO_2 distributions.

3. Results

Fig. 3 shows ~1000 subpolar NO_2 profiles for September and October for the SAGE3m observations and WACCM model simulations, as well as their relative frequencies of NO_2 concentrations in the UTLS (164–72 hPa). It is evident that SAGE3m and WACCMhet NO_2 abundances are broadly consistent. Note the occurrence of a substantial number of low values of NO_2 from ~50 hPa down to near the tropopause in both observations and model results, although it is more apparent in the model where values can be lower than 10 pptv (likely below the detection limit of the SAGE3m instrument, which reports an expected precision of 10%). For this reason, we are less interested in the extreme low values of NO_2 and more interested in the values near 50–100 pptv, which are within the measurement range of good estimated accuracy of the observations. In particular, SAGE3m and WACCMhet have a similar proportion of retrievals with $NO_2 < 100$ pptv (8% and 7%, respectively). On the other hand, less than 1% of SAGE3m NO_2 retrievals are less than 25 pptv, while 3% of the WACCMhet retrievals show NO_2 concentrations below 25 pptv. Comparison of Fig. 3b (WACCMhet) and Fig. 3d (WACCMnoHet) shows a stark change in NO_2 abundances based on the inclusion of heterogeneous chemical processes. In the 164–72 hPa region,

the mean NO_2 abundance for WACCMhet (317 pptv) is within 1% of the mean for the SAGE3m observations (318 pptv), while the mean for WACCMnoHet (359 pptv) is about 13% higher than the observed mean. The absence of low NO_2 abundances in WACCMnoHet (Fig. 3d; < 1% below 100 pptv NO_2, no retrievals with < 25 pptv NO_2) relative to observations (Fig. 3a) and WACCMhet (Fig. 3b) is a direct indication of heterogeneous halogen activation in this region. As more NO_2 in halogen nitrates is converted to HNO_3, this not only depletes NO_2, but it also increases the availability of ClO there and can deplete ozone, making such observations of NO_2 an important indicator for chemistry related to ozone depletion. Indeed, average NO_2 abundances in the 50–100 pptv range are much closer (and lower) for SAGE3m and WACCMhet than WACCMnoHet (78, 80, and 89 pptv, respectively).

Fig. 3e shows the PDF approach: we first collect all the data points for sampled profile observations and model simulations between 164 hPa and 72 hPa, as in the region denoted in Figs. 3a–d in the heart of the heterogeneous activation. The relative frequencies are constructed in 25 pptv bins. The observations (black) and model results with heterogeneous chemistry (blue) are overall in very good agreement. For 25–100 pptv, the normalized frequencies are lower in WACCMhet (0.04) relative to the observations (0.07). On the other hand, the model suggests a higher frequency (0.03) of occurrence of values below 25 pptv than the data (0.01). Again, instrument sensitivity may be an issue in terms of observation of these very low NO_2 concentrations.

The WACCMnoHet simulation PDF exhibits a large decrease in the probability of NO_2 values less than 125 pptv, compared to both the observed and WACCMhet PDFs (Fig. 3e). This is a qualitative but clear indication that heterogeneous activation is indeed occurring. Furthermore,

the observations and WACCMhet are in broad agreement. It is also important to note that there is a higher probability of NO_2 in the WACCMnoHet simulation in the higher magnitude NO_2 bins (relative to the WACCMhet simulation and observations). This is consistent with more available NO_2 shifting the distribution towards 200 pptv and higher. These results are not sensitive to the model horizontal resolution, as WACCMhet simulations at 1º yield almost identical distributions (Fig. S2).

Though we have excluded retrievals inside the polar vortex, the vortex edge at these altitudes is not as efficient a barrier to transport and mixing of polar and subpolar air as at higher altitudes (McIntyre, 1995), and so the chemical composition of subpolar air at these latitudes is subject to greater exchange between polar and midlatitude air (Tuck, 1989). Therefore, the denoxification in the LS in Figure 3 is due to a combination of heterogeneous activation outside the polar vortex and chemical processing inside and subsequent transport outside of the polar vortex. This is illustrated in Figs. 3c, e: WACCMnoHet60NS shows lower frequencies of NO_2 concentrations below 100 pptv and higher frequencies of concentrations in the 100–200 pptv concentration, relative to WACCMHet.

For a more quantitative comparison of the NO_2 distributions, Fig. 2 shows the ECDFs for the observations and three model simulations. The vertical lines indicate the maximum distances between each of the distributions, which is equivalent to the K–S test statistic. It is clear that the WACCMnoHet distribution (red) is different from the others, with the null hypothesis of the K–S test being rejected at the $\alpha = 0.00001$ level in all three cases (that is, the probability of WACCMnoHet NO_2 being drawn from the same distribution as SAGE3m (black), WACCMhet (blue), or WACCMnoHet60NS (green) is $p < 0.00001$). On the other hand, SAGE3m and

WACCMhet NO_2 are drawn from the same distribution, with the K–S test failing to reject the null hypothesis at the $\alpha = 0.05$ level. WACCMnoHet60NS is drawn from the same distribution as WACCMhet at the $\alpha = 0.1$ level, indicating that much of the heterogeneous activation evidenced by low NO_2 concentrations in WACCMhet is occurring at subpolar latitudes. However, WACCMnoHet60NS is drawn from a different distribution than SAGE3m: the null hypothesis is rejected with $p < 0.00001$; this further indicates that the exchange of polar-processed air with midlatitude air also contributes to the SAGE3m observed and WACCMhet NO_2 distributions.

In contrast to the clear heterogeneous halogen activation illustrated by the NO_2 distributions in the lower stratosphere, Fig. 4 shows the PDFs for the middle stratosphere (11–5 hPa), where heterogeneous chemistry is not expected to impact NO_2 concentrations. In this case, the WACCMhet and WACCMnoHet distributions are nearly identical (Fig. 4a–b), with the K–S test failing to reject the null hypothesis at the $\alpha = 0.5$ level. On the other hand, the SAGE3m NO_2 concentrations are clearly drawn from a different distribution than the model NO_2 concentrations, given the discrepancies in Figs. 4a–b. However, visual inspection reveals that the shapes of the distributions are very similar, and the differences reflect an offset. This stands in contrast to the differences in shape of the distributions found at lower altitudes between the observations and the WACCMnoHet case. Thus, we suggest that it is most likely that a model–observation bias of ~570 pptv (or ~9%) is responsible for these apparently "different" distributions. To demonstrate this, Figs. 4c–d show the same distributions with the WACCM NO_2 adjusted to have the same mean values as the SAGE3m observations by adding the mean difference to each WACCM profile. In this case, the three distributions are equal, with the K–S test failing to reject the null hypothesis at the $\alpha = 0.25$ level for WACCMhet–SAGE3m, and at the $\alpha = 0.5$ level for WACCMnoHet–SAGE3m. This is an important consideration, since it shows that the scales

(i.e., the spreads of the distributions) are alike, and it is the locations (i.e., the means) that cause the NO_2 distributions to be considered different at these levels. The bias was calculated as the difference between the means in this region, but the results are indifferent to different methods, such as scaling by the average difference between the observed and modelled profiles. This is in contrast to the UTLS region (Figs. 2–3), for which the SAGE3m observations and WACCMnoHet simulation are deemed to be drawn from different distributions ($p < 0.00001$), even after adjusting the means as above (Fig. S3).

4. Summary and Conclusions

Much deserved attention has been given to understanding the role of PSC heterogeneous halogen chemistry in driving changes in polar atmospheric composition and ozone depletion. In addition, important evidence has been presented for heterogeneous halogen chemistry outside the polar vortices (Santee et al., 2011; Thornton et al., 2003), but its scope and impacts have not been probed. In this study, we have identified substantial and consistent occurrence of such chemistry outside the polar regions, which broadens the scope of potential impacts associated with the chemistry of the subpolar stratosphere. While quantitative uncertainties remain (such as incomplete knowledge of thermal fluctuations potentially associated with sub-grid scale gravity waves, and of the rates of heterogeneous kinetic processes measured in the laboratory, etc.), the approach of analyzing probability distribution functions from models and satellite observations has been shown to provide an improved picture of key aspects of this chemistry.

In particular, we have shown that: (1) there is strong evidence for considerable heterogeneous halogen activation occurring locally in the subpolar lower stratosphere in September–October, as illustrated by the occurrence of extremely low NO_2 concentrations in the

observations and WACCMhet; (2) concentrations of NO_2 from observations and model simulations with heterogeneous chemistry turned on are drawn from the same distribution, and the inclusion of heterogeneous chemistry at both subpolar and polar latitudes appears to be *essential* for model–observation agreement; (3) at higher altitudes, where there is no heterogeneous activation, the model simulations with and without heterogeneous chemistry are nearly identical, and show the same scale (spread) as the observations, though the mean of the observations is about 9% higher than the model.

These results indicate that heterogeneous activation of halogens could play a role in ozone variability and trends in the subpolar lower stratosphere that is thus-far unaccounted for. WACCMnoHet60NS subpolar ozone abundances in the 164–72 hPa region are on average 4% lower than those for WACCMnoHet. It also highlights the importance of examining not only the mean state of atmospheric composition, but also its distribution. Impacts of heterogeneous processes in the modelled NO_2 abundances are evident in this region throughout the year. However, we focus here on September–October because of the density of observations in the subpolar region for this time period. Overall, these results act to enhance understanding of heterogeneous chemical processes and their impacts in the stratosphere.

Acknowledgments. BZ and DK were funded in part by NASA grant (80NSSC19K0952). BZ and SS were funded in part by NSF 1906719. This research was enabled by the computational and storage resources of NCAR's Computational and Information Systems Laboratory (CISL), sponsored by the NSF. Cheyenne: HPE/SGI ICE XA System (NCAR Community Computing). Boulder, CO: National Center for Atmospheric Research. https://doi.org/10.5065/D6RX99HX

Data Availability. Model output used is available at https://doi.org/10.7910/DVN/PIYPBB. MERRA2 reanalysis data are available at https://disc.gsfc.nasa.gov/datasets?keywords=%22MERRA-2%22&page=1&source=Models%2FAnalyses%20MERRA-2. SAGE satellite data is available at https://eosweb.larc.nasa.gov/project/sage3/sage3_table.

References

Adams, C., Bourassa, A. E., McLinden, C. A., Sioris, C. E., Clarmann, T. V., Funke, B., Rieger, L. A., & Degenstein, D. A. (2017). Effect of volcanic aerosol on stratospheric NO_2 and N_2O_5 from 2002–2014 as measured by Odin-OSIRIS and Envisat-MIPAS. *Atmos. Chem. Phys.*, *17*(13), 8063–8080. https://doi.org/10.5194/acp-17-8063-2017

Anderson, J. G., Wilmouth, D. M., Smith, J. B., & Sayres, D. S. (2012). UV dosage levels in summer: Increased risk of ozone loss from convectively injected water vapor. *Science*, *337*, 835–839. https://doi.org/10.1126/science.1222978

Anderson, J. G., Weisenstein, D. K., Bowman, K. P., Homeyer, C. R., Smith, J. B., Wilmouth, D. M., Sayres, D. S., et al. (2017). Stratospheric ozone over the United States in summer linked to observations of convection and temperature via chlorine and bromine catalysis. *Proc. Nat. Acad. Sci.*, *114*, E4905–E4913. https://doi.org/10.1073/pnas.1619318114

Barrera, J. A., Fernandez, R. P., Iglesias-Suarez, F., Cuevas, C. A., Lamarque, J. –F., & Saiz-Lopez, A (2020). Seasonal impact of biogenic very short-lived bromocarbons on lowermost stratospheric ozone between 60ºN and 60ºS during the 21st century. *Atmos. Chem. Phys.*, *20*, 8083–8102. https://doi.org/10.5194/acp-20-8083-2020

Borrmann, S., Solomon, S., Dye, J. E., & Luo, B. (1996). The potential of cirrus clouds for heterogeneous chlorine activation. *Geophys. Res., Lett.*, *23*(16), 2133–2136.

Chu, W. P., Trepte, C. R., Veiga, R. E., Cisewki, M. S., & Taha, G. (2002). SAGE III measurements, *Proc. SPIE*, *4814*. https://doi.org/10.1117/12.451515

Danabasoglu, G., Lamarque, J.□F., Bacmeister, J., Bailey, D. A., DuVivier, A. K., Edwards, J., et al. (2020). The Community Earth System Model Version 2 (CESM2). *Journal of Advances in Modeling Earth Systems*, *12*, e2019MS001916. https://doi.org/10.1029/2019MS001916

Epanechnikov, V. A. (1968). Non-parametric estimation of a multivariate probability density. *Theory Probab. Appl.*, *14*(1), 153–158. https://doi.org/10.1137/1114019

Fahey, D. W., Kawa, S. R., Woodbridge, E. L., Tin, P., Wilson, J. C., Jonsson, H. H., Dye, J. E., et al. (1993). Heterogeneous chemistry in the mid-latitude lower stratosphere: The role of reactive nitrogen and the impact of volcanic aerosol in ozone photochemistry. *Nature*, *363*, 509–514.

Gelaro, R., McCarty, W., Suárez, M. J., Todling, R., Molod, A., Takacs, L., et al. (2017). The Modern-Era Retrospective Analysis for Research and Applications, Version 2 (MERRA-2). *Journal of Climate*, *30*(14), 5419–5454. https://doi.org/10.1175/JCLI-D-16-0758.1

Gettelman, A., Mills, M. J., Kinnison, D. E., Garcia, R. R., Smith, A. K., Marsh, D. R., et al. (2019). The whole atmosphere community climate model version 6 (WACCM6). *Journal of Geophysical Research: Atmospheres*, *124*, 12,380–12,403. https://doi.org/10.1029/2019JD030943.

Hanson, D. R., Ravishankara, A. R., & Solomon, S. (1994). Heterogeneous reactions in sulfuric acid aerosols: A framework for model calculations. *J. Geophys. Res.*, *99*(D2), 3615-3629.

Lelieveld, J., Bregman, A., Scheeren, H. A., Strom, J., Carslaw, K. S., Fischer, H., Siegmund, P. C., & Arnold, F. (1999). Chlorine activation and ozone destruction in the northern lowermost stratosphere. *J. Geophys. Res.*, *104*(D7), 8201–8213.

Lin, S. J., & Rood, R. B. (1997). An explicit Flux-Form Semi-Lagrangian shallow water model on the sphere. *Quarterly Journal of the Royal Meteorological Society*, *123*, 2477–2498.

Mauldin, L., Salikhov, R., Habib, S., Vladimirov, A., Carraway, D., Petrenko, G., & Comella, J. (1998). Meteor-3M(1)/Stratospheric Aerosol and Gas Experiment III (SAGE III): Jointly

Sponsored by the National Aeronautics and Space Administration and the Russian Space Agency. *Proc. SPIE*, *3501*, 355–365.

Nash, E. R., Newman, P. A., Rosenfield, J. E., & Schoeberl, M. R. (1996). An objective determination of the polar vortex using Ertel's potential vorticity. *J. Geophys. Res.*, *101*(D5), 9471–9478. https://doi.org/10.1029/96JD00066

Sakazaki, T., Shiotani, M., Suzuki, M., Kinnison, D. E., Zawodny, J. M., McHugh, M., & Walker, K. A. (2015). Sunset–sunrise difference in solar occultation ozone measurements (SAGE II, HALOE, and ACE–FTS) and its relationship to tidal vertical winds. *Atmos. Chem. Phys.*, *15*, 829-843. https://doi.org/10.5194/acp-15-829-2015

Santee, M. L., Manney, G. L., Livesey, N. J., Froidevaux, L., Schwartz, M. J., & Read, W. G. (2011). Trace gas evolution in the lower stratosphere from Aura Microwave Limb Sounder measurements. *J. Geophys. Res.*, *116*, D18306, https://doi.org/10.1029/2011JD015590

Solomon, S., Borrmann, S., Garcia, R. R., Portmann, R., Thomason, L., Poole, L. R. Winker, D., & McCormick, M. P. (1997). Heterogeneous chlorine chemistry in the tropopause region. *J. Geophys. Res.*, *102*, 21411–21429.

Solomon, S. (1999). Stratospheric ozone depletion: A review of concepts and history. *Rev. Geophys.*, *37*, 275–316. https://doi.org/10.1029/1999RG900008

Solomon, S., Kinnison, D., Bandoro, J., & Garcia, R. R. (2015). Polar ozone depletion: An update. *J. Geophys. Res. Atmos.*, *120*, 7958–7974. https://doi.org/10.1002/2015JD023365

Solomon, S., Kinnison, D. E., Garcia, R. R., Bandoro, J., Mills, M., Wilka, C., Neely III, R. R., et al. (2016). Monsoon circulations and tropical heterogeneous chlorine chemistry in the stratosphere. *Geophys. Res. Lett.*, *43*(24), 12,624–12,633. https://doi.org/10.1002/2016GL071778

Solomon, S., Ivy, D., Gupta, M., Bandoro, J., Santer, B., Fu, Q., Garcia, R. R., et al. (2017). Mirrored changes in Antarctic ozone and stratospheric temperature in the late 20th versus early 21st centuries. *J. Geophys. Res*. https://doi.org/10.1002/2017/JD026719

Smirnov, N. (1948). Table for estimating the goodness of fit of empirical distributions. *Annals of Mathematical Statistics*, *19*(2), 279–281. https://doi.org/10.1214/aoms/1177730256

Thornton, B. F., Toohey, D. W., Avallone, L. M., Harder, H., Martinez, M., Simpas, J. B., Brune, W. H., & Avery, A. M. (2003). In situ observations of ClO near the winter polar tropopause. *J. Geophys. Res.*, *108*(D8), 8333. https://doi.org/10.1029/2002JD002839

Waugh, D. W., Sobel, A. H., & Polvani, L. M. (2017). What is the polar vortex and how does it influence weather? *Bull. Amer. Met. Soc.*, *98*(1), 37–44. https://doi.org/10.1175/BAMS-D-15-00212.1

Zambri, B., Solomon, S., Kinnison, D. E., Mills, M. J., Schmidt, A., Neely, R. R., III, et al. (2019). Modeled and observed volcanic aerosol control on stratospheric NO_y and Cl_y. *Journal of Geophysical Research: Atmospheres*, *124*. https://doi.org/10.1029/2019JD031111

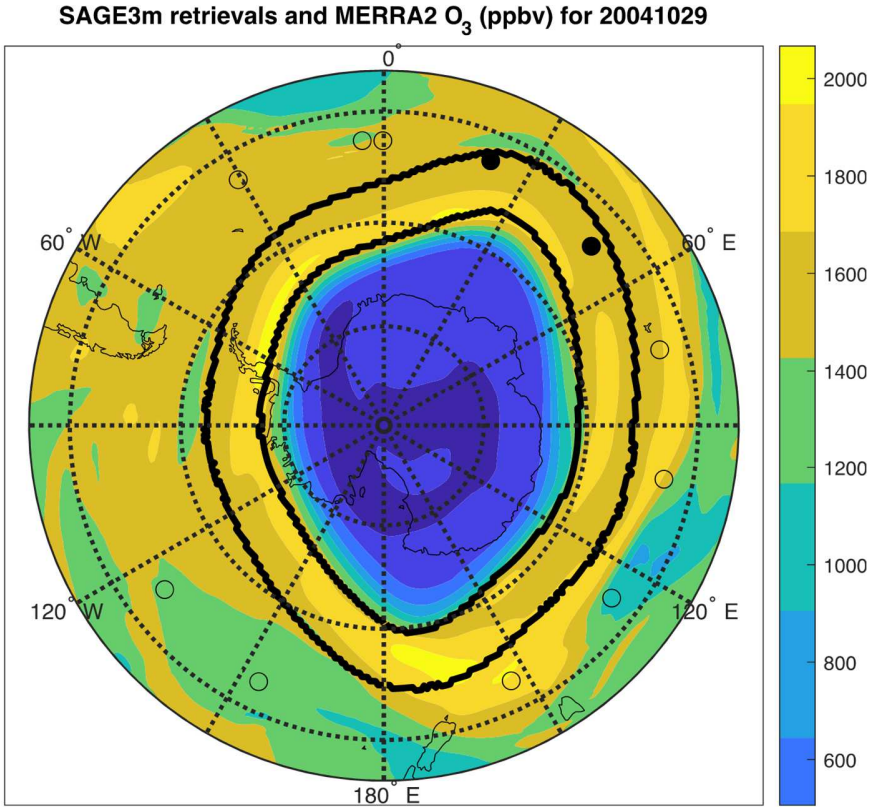

Figure 1. Locations of SAGE3m retrievals in the Southern Hemisphere for October 29, 2004 as an example. Open and filled circles represent retrievals that were excluded from and included in the analysis, respectively, based on proximity to the vortex edge. Black contours indicate the subpolar region as determined by the maximum PV gradient on the 460 K isentrope on that day. Also shown are the MERRA2 O_3 concentrations at 460 K, to highlight the changes in atmospheric composition inside and outside the polar vortex.

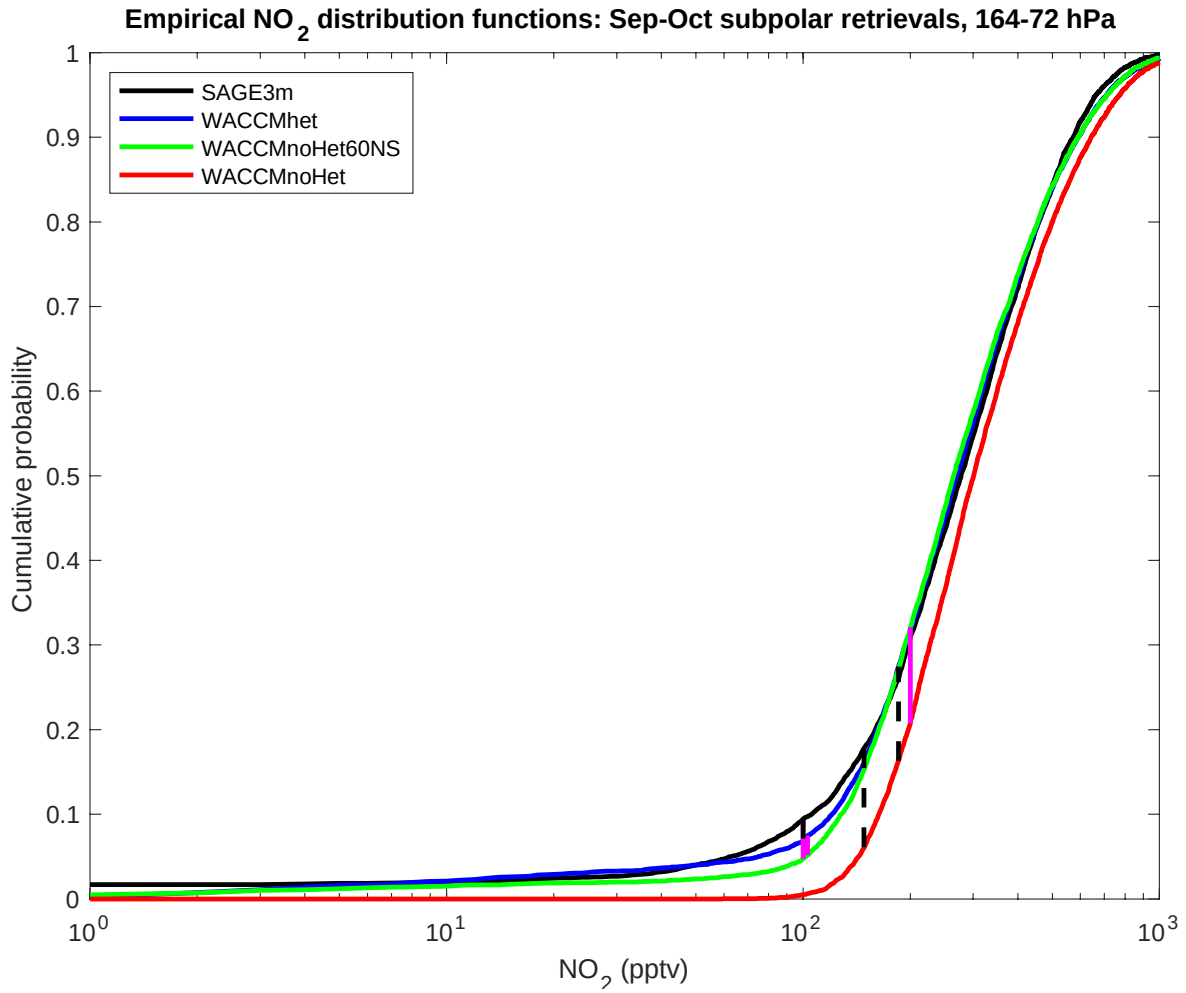

Figure 2. ECDFs for (black) SAGE3m, (blue) WACCMhet, (green) WACCMnoHet60NS, and (red) WACCMnoHet. Vertical dashed lines indicate the two-sample K–S test statistics, which are the maximum distances between two samples (magenta lines for WACCMnoHet60NS). Distribution functions shown are for September–October and 164–72 hPa.

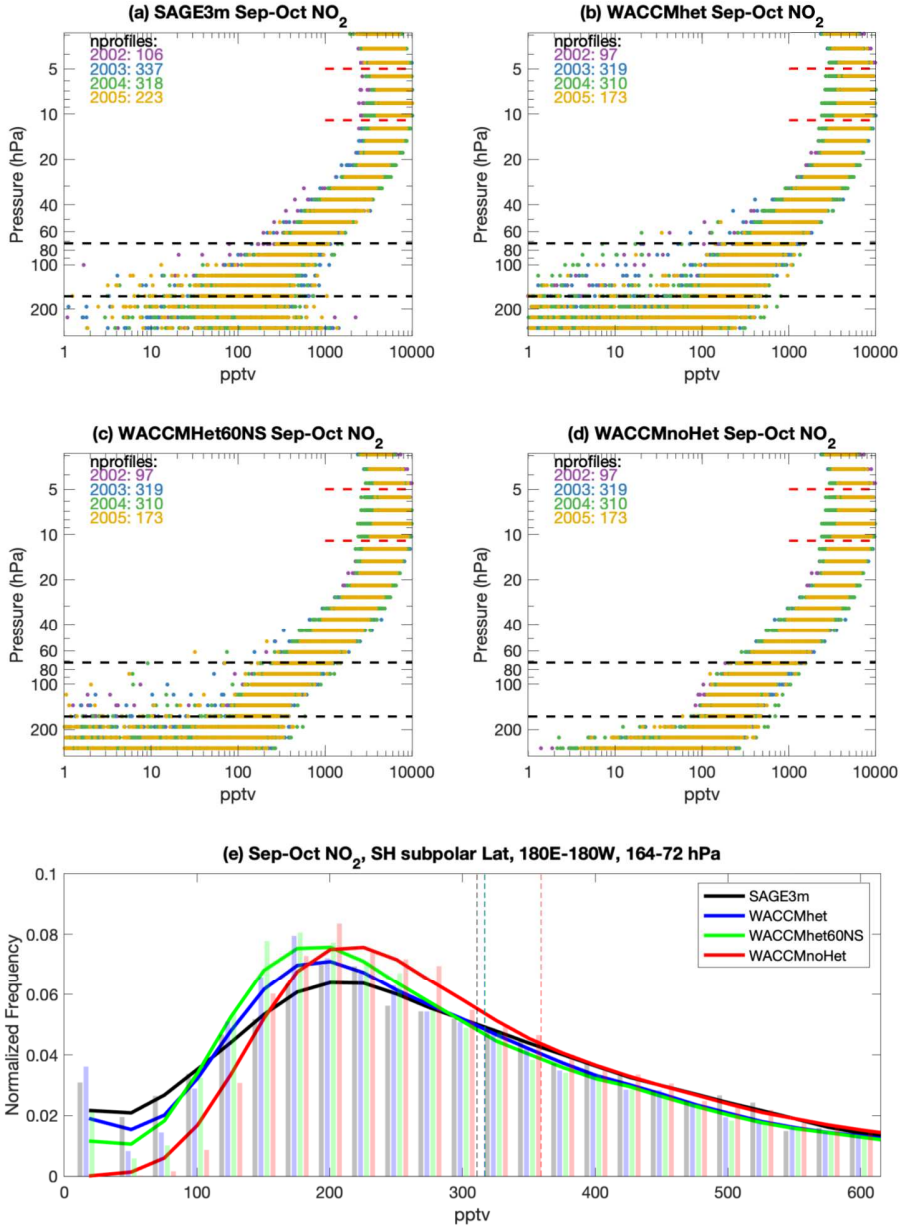

Figure 3. (a)–(d): September–October NO_2 concentrations for subpolar retrievals for (a) SAGE3m, (b) WACCMhet, (c) WACCMhet60NS, and (d) WACCMnoHet. (e) PDFs for 164–72 hPa for (black) SAGE3m, (blue) WACCMhet, (green) WACCMhet60NS, and (red) WACCMnoHet. Black horizontal dashed lines in (a)–(d) indicate the vertical range for the distributions in (e); red horizontal dashed lines indicate the vertical range for Fig. 4. Solid curves in (e) are the Epanechnikov kernel density estimates (Epanechnikov, 1968); dashed vertical lines

are the mean NO_2 values for each distribution. Nprofiles represents the number of profiles that lie inside the polar vortex region for a given year.

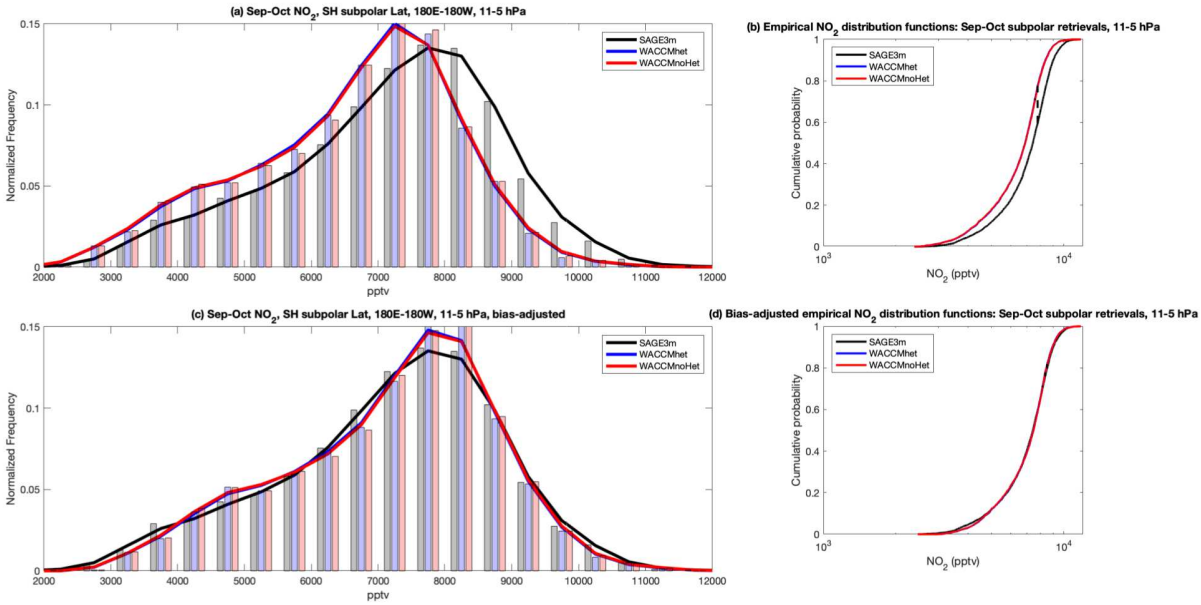

Figure 4. (a) PDFs and (b) ECDFs of September–October NO_2 concentrations for subpolar retrievals for 11–5 hPa for (black) SAGE3m, (blue) WACCMhet, and (red) WACCMnoHet. (c)–(d): as (a)–(b), but with WACCM means adjusted to match the SAGE3m mean.